Bioorganic Chemistry 57 (2014) 155–161

Contents lists available at ScienceDirect

Bioorganic Chemistry

journal homepage: www.elsevier.com/locate/bioorg

Synthesis of azobenzenealkylmaleimide probes to photocontrol the enzyme activity of a bacterial histone deacetylase-like amidohydrolase

Benjamin Horstmann [a,1], Michael Korbus [a,1], Tatjana Friedmann [a], Christiane Wolff [b], Christina Marie Thiele [b], Franz-Josef Meyer-Almes [a,*]

[a] Department of Chemical Engineering and Biotechnology, University of Applied Sciences Darmstadt, 64287 Darmstadt, Germany
[b] Clemens-Schöpf Institute of Organic Chemistry and Biochemistry, Technical University of Darmstadt, 64287 Darmstadt, Germany

ARTICLE INFO

Article history:
Received 6 August 2014
Available online 24 October 2014

Keywords:
Deacetylation
External stimulus
Photochromism
Protein engineering
Photoswitch
Azobenzenes
Maleimides
Methylenemaleimideamide
Hofmann rearrangement

ABSTRACT

A series of azobenzenealkylmaleimides (AMDs) with different spacer length was synthesized and coupled *via* Michael-Addition to a specific mutant of a bacterial histone deacetylase-like amidohydrolase (HDAH). Michaelis–Menten parameters (V_{max} and K_m) were employed to characterize the effect of both, the spacer length and the configuration (*cis* vs. *trans*) of the attached azobenzene moiety, on the HDAH enzyme activity. The photoswitch behavior of the AMD/enzyme conjugate activity was clearly influenced by the AMD spacer length. This study highlights the importance of steric rearrangement of the photoswitch with respect to the active site and describes a strategy to optimize the photocontrol of HDAH.

1. Introduction

Bioconjugation of light-switchable molecules is a widely used method to introduce stimulus sensitive moieties to biomolecules [1–3]. The isomerization process of light-responsive molecules offers diversified applications like photocontrol of the protein function [4–8] or the conformational change of protein structures [9,10] as well as protein assembly [11]. Azobenzene is the most studied light-switchable molecule. It undergoes a reversible isomerization process from the *E*- to the *Z*-isomer by irradiating with UV-light. The back-isomerization to the lower energy *E*-isomer (*trans*) can be realized by visible light (vis) or by thermal relaxation [12,13]. In addition to the configuration, the polarity of the azobenzene group is also switched. Both factors play an important role if azobenzene containing molecules are covalently bound to a protein surface. Bioconjugation of small molecules requires mild conditions and an orthogonal coupling strategy whereupon the Michael-Addition towards the thiol group of cysteine residues fulfills these conditions [14]. The variation of linker length is a common motif to probe the influence of a specific group to a defined area [15,16]; this elongation can be achieved by the use of different diamines. These advantages were combined by the synthesis of a series of new azobenzenealkylmaleimides (AMDs) **1a–e**. Subsequently, the reactive probes were conjugated to a specific cysteine-variant (M30C) of a photoswitchable bacterial histone deacetylase-like amidohydrolase (HDAH) from *Bordetella/Alcaligenes* strain FB188 [7] to investigate the influence of AMD spacer length variation as well as the *cis*- and *trans*-configuration on the photocontrol behavior of the enzyme activity. Furthermore, spatio-temporal controlled deacetylation reactions could be employed in biotechnological and biomedical applications to regulate the deacetylation of biomolecules or chemical compounds in a precise and defined manner to meet desired needs.

2. Materials and methods

2.1. General methods

All chemical reagents were of analytical grade, obtained from commercial suppliers and used without further purification. THF was freshly distilled under argon from sodium and stored over sodium and under argon atmosphere. TEA was distilled and stored over KOH. Column chromatography was carried out on silica gel 60 (40–60 μm), Macherey-Nagel. Reactions and chromatography

* Corresponding author.
E-mail address: franz-josef.meyer-almes@h-da.de (F.-J. Meyer-Almes).
[1] First author.

http://dx.doi.org/10.1016/j.bioorg.2014.10.004
0045-2068/

fractions were analyzed on precoated silica gel plates (silica gel 60, F254, 20 × 20 cm, 0.25 mm thick, Merck thin-layer chromatography). Amino and Boc protected amino groups were stained by dipping the TLC plate in a ninhydrin solution (0.66% m/v in EtOH) following by heating or by absorbance of UV light at 254 nm. NMR-spectra were recorded with an Avance 300 (AC300) (300 MHz ^{1}H, 75 MHz ^{13}C) and a Bruker DRX 500 (500 MHz ^{1}H, 126 MHz ^{13}C)-spectrometer. The chemical shift data for each signal is given in units of δ (ppm) relative to tetramethylsilane (TMS), assigned δ (TMS) = 0. Coupling constants (J) are stated in Hz. HPLC–MS was performed with an Agilent Technologies Series 1200 instrument using an Agilent Eclipse XDB-C18 column. Method: 5–95% B from 2 to 17 min, 95–5% B from 20 to 25 min. Solvent A: water + 0.1% formic acid; solvent B: acetonitrile + 0.1% formic acid. The *cis*- and *trans* photoisomerization of AMDs (**1a–e**) conjugated to HDAH variant M30C was verified by UV/Vis spectroscopy measurements in MC buffer (40 mM sodium phosphate, 150 mM NaCl, 1 mM EDTA, pH 7.2) at 30 °C. A solution of 3 μM of the respective AMD/HDAH M30C conjugate was irradiated by UV light by use of a hand lamp (6 W, Heraeus) at 364 nm for 25 min at a distance of 6 cm (43 mJ cm^{-2}) or blue light (1 W, LED, Osram) at 464 nm for 25 min at a distance of 6 cm (1.5 J cm^{-2}) to achieve the *cis*- or *trans*-configuration. UV/Vis spectra (280–400 nm) of photoisomerized samples were subsequently recorded with a UV/Vis spectrophotometer (Jasco V-630).

2.2. Biochemical methods

2.2.1. Employed HDAH variants

HDAH variant C51S was used to investigate the inhibitory effect of the respective *cis*- and *trans*-configuration of (*E*)-1-(4-(phenyldiazenyl)phenyl)-1*H*-pyrrole-2,5-dione (4-PAM) and AMDs (**1a–e**) by determination of IC_{50} values. HDAH variant M30C was used as conjugate and test model to investigate the AMD dependent influence on the photoswitch capability with respect to the spacer length. Both HDAH variants were generated by site-directed mutagenesis, expressed in *Escherichia coli* strain XL1-blue and purified as previously reported [7].

2.2.2. Modification of HDAH variant M30C

The single solvent accessible cysteine of HDAH variant M30C was chemically modified by 4-PAM or AMDs (**1a–e**) by a 4-fold molar excess in MC buffer (supplemented with 8% DMSO) and the modification procedure continued as described previously [7].

2.2.3. Determination of Michaelis–Menten kinetics

The determination and analysis of Michaelis–Menten kinetics of unmodified and AMD (**1a–e**) modified HDAH M30C variants, photoisomerized to their *cis*- (UV light, 364 nm, 43 mJ cm^{-2}) and *trans*-configuration (blue light, 464 nm, 1.5 J cm^{-2}), was performed as reported previously [7]. Pluronic F 68 was purchased from BASF and bovine serum albumin from Sigma–Aldrich. Measurements were performed as independent triple measurements and Michaelis–Menten parameters (K_m and V_{max}) represented as means ± standard deviation (SD), n = 3. The photoswitch efficiency of V_{max}- and K_m-values, between the *cis*- and *trans*-configuration, was calculated as percentages by definition of the more active isomer.

2.2.4. DOL value determination

The DOL value (average number of conjugated AMD molecules per each HDAH variant M30C molecule) calculation of AMD/HDAH M30C variant conjugates was performed as described previously [7] *via* Lambert–Beer equation by use of the determined molar extinction coefficient (ε) of *trans* 4-PAM at its absorbance maximum after conjugation to HDAH variant M30C (15,700 l mol^{-1} cm^{-1}; 330 nm) and the predicted ε of HDAH wild type (wt) (43,890 l mol^{-1} cm^{-1}; 280 nm).

2.2.5. Determination of IC_{50} values

To determine the inhibitory effect of the *cis*- and *trans*-configuration of 4-PAM and AMDs (**1a–e**) on HDAH variant C51S activity, dose–response curves were performed and IC_{50} values analyzed. The HDAH C51S activity was determined by employing a fluorescence-based activity assay in a similar way as described previously [17,18]. 5 mM 4-PAM or AMD (**1a–e**) DMSO solutions were isomerized to their *cis*-configuration by UV light irradiation (364 nm, 43 mJ cm^{-2}) using a hand lamp as described before and serially diluted in FB188 buffer (15 mM Tris, 50 mM KH_2PO_4/K_2HPO_4, 250 mM NaCl, 250 μM EDTA, 0.001% Pluronic F 68 and 0.005% bovine serum albumin; pH 8.0). The *trans*-configuration of mentioned compounds was achieved by thermal relaxation of the serially diluted samples due to incubation at 30 °C for 5 h in the dark. The HDAH catalyzed deacetylation reaction, in dependence on increasing 4-PAM or AMD concentrations, was performed as a one-step assay in the dark in black 96-well half-area microplates (flat bottom, polystyrene, medium binding; Greiner Bio-One) providing final concentrations of 100 nM HDAH variant C51S, 0.5 mg/mL Trypsin from bovine pancreas (Serva) and 50 μM BocLys(Ac)AMC (Bachem) as substrate. The fluorescence intensity of 7-amino-4-methylcoumarin (AMC) was detected at 450 nm (350 nm excitation) over a period of 2 h at 30 °C and the HDAH C51S activity determined from the slope of the linear initial phase of measured kinetics and expressed as relative fluorescence units per second (RFU s^{-1}). The latter was correlated to the activity of a sample of HDAH C51S where no compound was added (stated as 100%), the activity expressed as percentages and plotted against the log of applied compound concentration. Dose–response curves were analyzed by the program GraphPad Prism (GraphPad Software) using a three-parameter dose–response model and IC_{50}-values determined in independent triplicates and specified as means ± SD, n = 3. Dose–response curves of DMSO were equally determined as described before using HDAH-wt to verify the real inhibitory effect, induced by 4-PAM and AMDs (**1a–e**) on HDAH activity. Additionally, a dose–response curve of a known histone deacetylase inhibitor like suberoylanilide hydroxamic acid (SAHA) was tested on HDAH-wt activity to compare the inhibitory potency with 4-PAM and AMDs. The dose–response curve of SAHA was performed as a single determination by use of the above described assay conditions and data points comparably analyzed by a three-parameter dose–response model.

3. Experimental procedure

3.1. Synthesis of AMD 1b–e

The procedure of the synthesis of compounds **3c–e, 4c–e, 5c–e** and **7** as well as the ^{1}H NMR and ^{13}C NMR spectra of AMDs **1a–e** can be found in supplementary material.

3.1.1. (E)-N-(2-(2,5-dioxo-2,5-dihydro-1H-pyrrol-1-yl)ethyl)-4-(phenyldiazenyl)benzamide (**1b**)

To a solution of 1-(2-aminoethyl)-1*H*-pyrrol-2,5-dione 2,2,2-hydrochloride: (150 mg, 0.849 mmol) and TEA (350 μL, 2.50 mmol) in THF (4 mL) was added (*E*)-perfluorophenyl 4-(phenyldiazenyl)benzoat **7** (666 mg, 1.70 mmol) in THF (4 mL) dropwise. After 16 h at rt, the solvent was evaporated, the resulting residue was dissolved in $CHCl_3$ and washed with H_2O (30 mL), 1 M HCl (30 mL) and brine (30 mL). The organic layer was dried over Na_2SO_4, filtered and concentrated. The crude product was purified by silica column (eluent EtOAc:hexane: 1:4 → 1:1; R_f: 0.10 → 0.50)

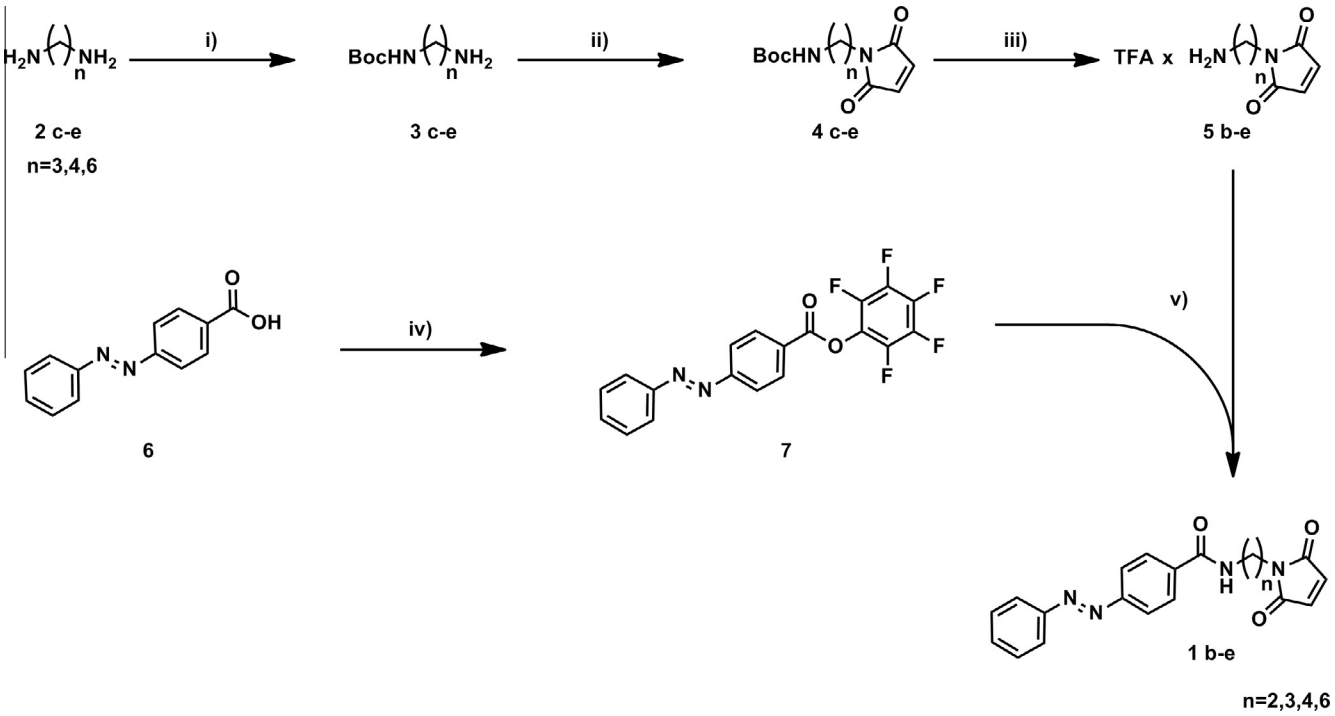

Scheme 1. Reaction scheme for the synthesis of AMDs **1b–e**: (i) Boc_2O, DCM; (ii) 1. Maleic anhydride, DCM; 2. Ac_2O, NaOAc, 65 °C, 3 h; (iii) DCM:TFA (2:1); (iv) perfluorophenyl 2,2,2-trifluoroacetate, THF; (v) TEA, THF. Commercial available 1-(2-aminoethyl)-1*H*-pyrrole-2,5-dione hydrochloride (**5b**) was used for the synthesis of **1b**.

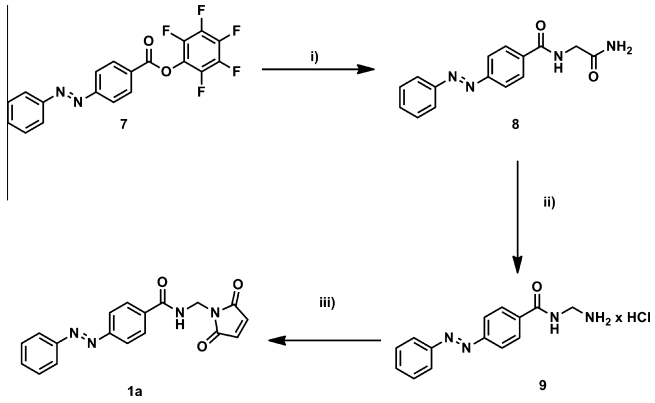

Scheme 2. Reaction scheme for the synthesis of the geminal amidomaleimide **1a**: (i) glycineamide hydrochloride, DMF, TEA; (ii) PIFA, DMSO:H_2O (1:1); (iii) 1. Maleic anhydride, DIEA, DCM; 2. EDC, HOBt, DMF.

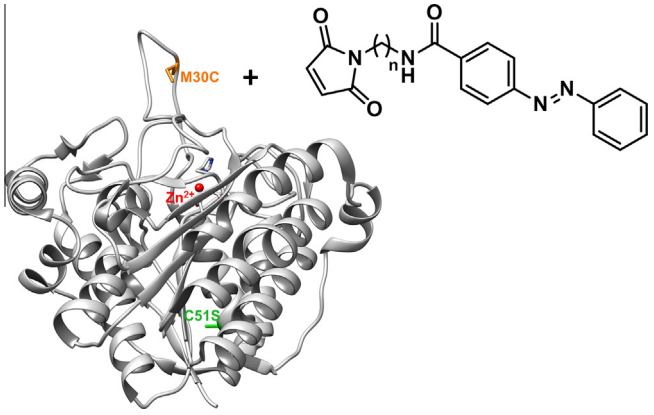

Fig. 1. Chemical modification of HDAH variant M30C by AMDs. HDAH variant M30C was employed as a conjugation model to investigate the effect of the alkyl spacer length (n = 1, 2, 3, 4 and 6) on the photoswitch capability of enzyme activity. AMDs (**1a–e**) were covalently conjugated to the mutated cysteine at amino acid position 30, which was original a methionine before (M30C, orange). The HDAH variant C51S, where a cysteine was substituted by serine, was used to test the inhibitory effect of AMDs by determination of IC_{50} values. The latter mentioned mutation was also present in HDAH variant M30C to ensure a precise modification of AMDs at the mentioned cysteine. The catalytic zinc ion (Zn^{2+}, red sphere) displays the active site which is complexed by one histidine (H182) and two aspartate residues (D180 and D268). The illustration of mutated cysteines is based on the X-ray crystal of HDAH-wt (PDB ID 2VCG, chain A, [24]). (For interpretation of the references to color in this figure legend, the reader is referred to the web version of this article.)

to yield the product as an orange solid (243 mg; 82%). ^{1}H NMR (500 MHz, DMSO) δ 8.73 (t, J = 6.0 Hz, 1H), 7.96–7.88 (m, 6H), 7.67–7.56 (m, 3H), 7.01 (s, 2H), 3.62 (t, J = 5.7 Hz, 2H), 3.45 (dd, J = 11.6, 5.9 Hz, 2H); ^{13}C NMR (126 MHz, DMSO) δ 171.04, 165.76, 153.24, 151.89, 136.61, 134.51, 131.92, 129.49, 128.35, 122.67, 122.27, 37.71, 37.10; HPLC/MS (t_r = 13.92 min; ESI) found: 349.1 $(M+H)^+$, calc.: 349.1.

*3.1.2. (E)-N-(3-(2,5-dioxo-2,5-dihydro-1H-pyrrol-1-yl)propyl)-4-(phenyldiazenyl)benzamide (**1c**)*

To a solution of 1-(4-aminopropyl)-1*H*-pyrrole-2,5-dione 2,2,2-trifluoracetat salt (**5c**) (608 mg, 2.28 mmol) and TEA (950 µL, 6.84 mmol) in THF (14 mL) was added dropwise (*E*)-perfluorophenyl 4-(phenyldiazenyl)benzoate (1.79 g, 4.56 mmol) in THF (14 mL). After 16 h at rt, the solvent was evaporated, the resulting residue was dissolved in $CHCl_3$ (200 mL) and washed with H_2O (100 mL), 1 M HCl (100 mL) and brine (100 mL). The organic layer was dried over Na_2SO_4, filtered and the solvent was removed under reduced pressure. The crude product was purified by column chromatography (EtOAc/hexane 1:1 → 6:4; R_f: 0.42) to obtain 41 mg (5%) of the desired compound. ^{1}H NMR (500 MHz, DMSO) δ 8.65 (t, J = 5.6 Hz, 1H), 8.15–7.89 (m, 6H), 7.68–7.59 (m, 3H), 7.04 (s, 2H), 3.51 (t, J = 7.2 Hz, 2H), 3.34–3.27 (m, 2H), 1.83 (p, J = 7.2 Hz, 2H); ^{13}C NMR (126 MHz, DMSO) δ 171.51, 165.91, 153.73, 152.43, 137.19, 135.00, 132.44, 130.02, 128.93, 123.19, 122.81,

37.51, 35.72, 28.52; HPLC/MS (t_r = 14.30 min; ESI) found: 363.2 $(M+H)^+$, calc.: 363.1.

*3.1.3. (E)-N-(4-(2,5-dioxo-2,5-dihydro-1H-pyrrol-1-yl)butyl)-4-(phenyldiazenyl) benzamide (**1d**)*

To a solution of 1-(4-aminobutyl)-1*H*-pyrrole-2,5-dione 2,2,2-trifluoracetate (**5d**) (104 mg, 0.370 mmol) and TEA (155 µL, 1.10 mmol) in THF (4 mL) was added dropwise (*E*)-perfluorophenyl 4-(phenyldiazenyl)benzoate (**7**) (289 mg, 0.740 mmol) in THF (3 mL). After 16 h at rt, the solvent was evaporated, the resulting residue was dissolved in $CHCl_3$ (40 mL) and washed with H_2O (20 mL), 1 M HCl (20 mL) and brine (20 mL). The organic layer was dried over Na_2SO_4, filtered and concentrated. Purification by silica column (eluent: EtOAc:hexane: 1:4 → 1:1; R_f: 0.10 → 0.40) afforded the product as an orange solid (56 mg; 45%). ^{1}H NMR (500 MHz, $CDCl_3$) δ 8.08–7.87 (m, 6H), 7.60–7.50 (m, 3H), 6.73 (s, 2H), 6.39 (*br* s, 1H), 3.62 (t, J = 6.9 Hz, 2H), 3.55 (dd, J = 12.6, 6.5 Hz, 2H), 1.81–1.62 (m, 4H); ^{13}C NMR (126 MHz, $CDCl_3$) δ 170.98, 166.97, 154.39, 152.73, 136.48, 134.28, 131.69, 129.30, 128.05, 123.22, 123.08, 39.78, 37.51, 26.84, 26.30; HPLC/MS (t_r = 14.56 min; ESI) found: 377.1 $(M+H)^+$, calc.: 377.1.

*3.1.4. 6-(2,5-dioxo-2,5-dihydro-1H-pyrrol-1-yl)hexyl-4-(phenyldiazenyl)-benzamide (**1e**)*

N-(6-aminohexyl)maleimide (85 mg, 283 µmol) was placed in a flask and dissolved in 1.4 mL THF and 125 µL TEA (900 µmol). (*E*)-perfluorophenyl 4-(phenyldiazenyl)benzoate (222 mg, 570 µmol) in 1.4 mL THF were added dropwise and the reaction stirred for 16 h. The solvent was removed, the residue was dissolved in 25 mL $CHCl_3$, washed with H_2O, 1 M HCl and brine. The organics were dried over Na_2SO_4, filtered and concentrated. The crude product was purified by silica column (eluent EtOAc:hexane: 1:4 → 1:1; R_f: 0.10 → 0.50) to yield the product as an orange solid (70 mg; 61%).^{1}H NMR (500 MHz, $CDCl_3$) δ 7.99–7.87 (m, 6H), 7.64–7.42 (m, 3H), 6.66 (s, 2H), 6.49 (br s, 1H), 3.51 (t, J = 7.1 Hz, 2H), 3.44 (dd, J = 13.0, 6.9 Hz, 2H), 1.67–1.55 (m, 4H), 1.46–1.38 (m, 2H), 1.35–1.29 (m, 2H); ^{13}C NMR (126 MHz, $CDCl_3$) δ 170.98, 166.92, 154.25, 152.66, 136.66, 134.15, 131.62, 129.24, 128.02, 123.16, 122.97, 40.02, 37.64, 29.52, 28.45, 26.30, 26.26; HPLC/MS (t_r = 15.55 min; ESI) found: 405.2 $(M+H)^+$, calc.: 405.2.

3.2. Synthesis of AMD 1a

*3.2.1. (E)-N-(2-amino-2-oxoethyl)-4-(phenyldiazenyl)benzamide (**8**)*

To a solution of 2-aminoacetamide hydrochloride (16.8 mmol, 1.86 g) in 84 mL DMF and TEA (4.67 mL, 33.8 mmol) was added a solution of the active ester **7** (2.20 g, 5.61 mmol) in 28 mL DMF. After 3 h the reaction mixture was extracted with $CHCl_3$. The organic layer was washed with sat. NH_4Cl solution and brine, dried over Na_2SO_4, filtered and concentrated. 200 mg of the desired compound could be obtained. To raise the yield, the not completely dissolved emulsion (obtained by extraction) was precipitated in hexane. The precipitates were filtered and dried. Overall 603 mg (38%) of the benzamide **8** could be obtained. ^{1}H NMR (500 MHz,

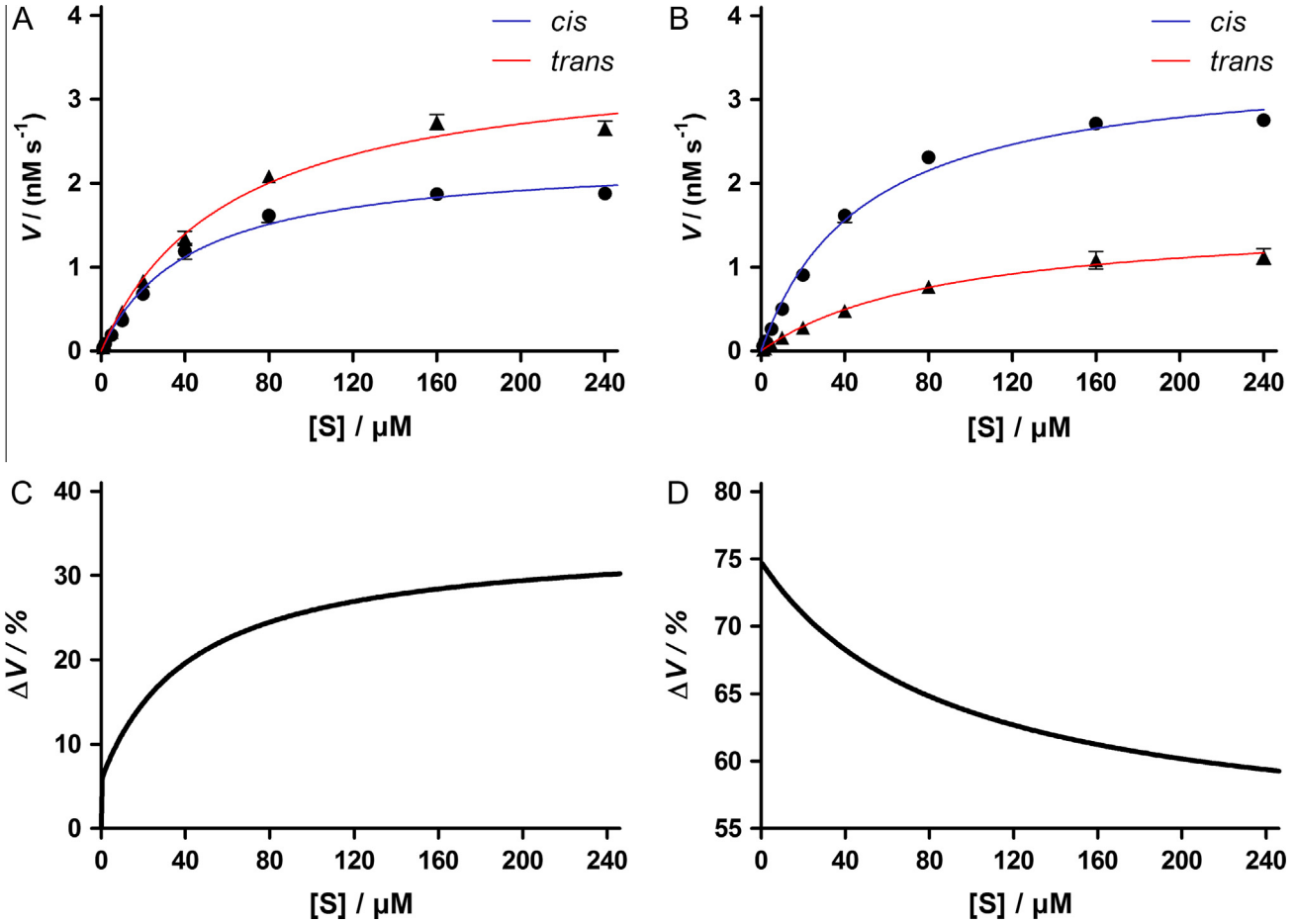

Fig. 2. Michaelis–Menten kinetics of AMD/HDAH M30C conjugates. HDAH M30C was covalently modified by AMD **1a** (A), **1b** (B) and the respective *cis*- and *trans*-configuration achieved by UV-(364 nm) or blue-light (464 nm) irradiation. (C) (for AMD-**1a**) and (D) (for AMD-**1b**) show the relative difference of the velocity value (*V*) between both configurations. If no error bars are detectable, SD values are so small that they are indistinguishable from most data points. (For interpretation of the references to color in this figure legend, the reader is referred to the web version of this article.)

DMSO) δ 8.88 (t, J = 5.9 Hz, 1H), 8.15–8.10 (m, 2H), 8.01–7.93 (m, 4H), 7.67–7.60 (m, 3H), 7.44 (s, 1H), 7.06 (s, 1H), 3.88 (d, J = 5.9 Hz, 2H); ^{13}C NMR (126 MHz, DMSO) δ 171.33, 166.11, 153.82, 152.43, 136.79, 132.46, 130.02, 129.16, 123.20, 122.77, 45.98; HPLC/MS (t_r = 14.01 min; ESI) found: 283.1 $(M+H)^+$, calc.: 283.1.

3.2.2. (E)-N-(aminomethyl)-4-(phenyldiazenyl) benzamide hydrochloride (**9**)

(Bis(trifluoroacetoxy) iodo)benzene (1.12 g, 2.73 mmol) was dissolved in 14 mL DMSO and 3.8 mL H_2O. Afterwards **8** was added and the mixture was stirred at rt for 16 h. The solution was subsequently poured in 1 M HCl and washed with Et_2O. The azobenzene compounds did not completely dissolve in the aqueous layer. The orange foam was taken and lyophilized to obtain 411 mg of a mixtures of **8** and **9** (44%:56%; n/n calculation *via* ^{1}H NMR; 38% yield for the **9**). ^{1}H NMR (300 MHz, DMSO) (selected data) δ 9.83 (t, J = 5.9 Hz, 1H), 8.42 (s, 3H), 8.19–8.07 (m, 2H), 8.06–7.88 (m, 4H), 7.68–7.55 (m, 3H), 4.44 (d, J = 6.0 Hz, 2H).

3.2.3. (E)-N-((2,5-dioxo-2,5-dihydro-1H-pyrrol-1-yl)methyl)-4-(phenyldiazenyl)benzamide (**1a**)

350 mg of a mixtures of **8** and **9** (0.685 mmol **9**) was dissolved in 16 mL DCM and 660 µL DIPEA. Maleic anhydride (159 mg; 1.62 mmol) was added and the mixture was stirred at rt for 4 h. Afterwards 15 mL 1 M HCl was added, the aqueous layer was separated and the not completely dissolved orange layer was precipitated in hexane and filtered to obtain 319 mg of an orange solid. The unpurified (*Z*)-4-oxo-4-(((4-((*E*)-phenyldiazenyl)benzamido) methyl)amino)but-2-enoic acid was dissolved in 15 mL DMF and was added dropwise to a solution of HOBt × H_2O (166 mg; 1.09 mmol), EDC × HCl (208 mg; 1.09 mmol) and DIPEA (371 µL; 2.17 mmol) in 50 mL DMF. After 16 h the reaction was concentrated to a volume of 10 mL, 50 mL $CHCl_3$ were added and the organic layer was washed with H_2O (3 times à 50 mL) and brine (30 mL), dried over Na_2SO_4, filtered and concentrated. The crude product was purified by silica column (eluent EtOAc:hexane: 1:1; R_f: 0.38) to yield the product as an orange solid (62 mg; 27%). ^{1}H NMR (500 MHz, DMSO) δ 9.16 (t, J = 5.1 Hz, 1H), 8.08–8.02 (m, 2H), 7.97–7.90 (m, 4H), 7.65–7.56 (m, 3H), 7.08 (s, 2H), 5.03 (d, J = 5.2 Hz, 2H); ^{13}C NMR (126 MHz, DMSO) δ 170.08, 165.28, 153.46, 151.89, 134.80, 131.99, 129.50, 128.72, 122.70, 122.29, 42.69; HPLC/MS (t_r = 14.01 min; ESI) found: 335.1 $(M+H)^+$, calc.: 335.1.

4. Results and discussion

4.1. Synthesis of AMDs

The synthesis procedure to achieve the desired AMDs is shown in Schemes 1 and 2. AMDs **1b–e** could be synthesized by starting with selective monoprotection of the corresponding diamine **2c–e**, followed by an introduction of the maleimide moiety over two steps. Maleic anhydride reacts with the primary amine followed by cyclisation. After removal of the Boc-group aminoalkylmaleimides **5b–e** were coupled to preactivated azobenzoic acid **7** to obtain AMD **1b–e**.

Due to the fact that monoprotected diaminomethane is not easily accessible [19,20] the reaction strategy for AMD **1a** had to be changed. The reaction of glycineamide hydrochloride with pentafluorophenyl 4-(2-phenyldiazenyl)benzoate **7** yielded the azobenzeneglycineamide **8**. The geminale aminoamide hydrochloride **9** was obtained by acetic Hofmann rearrangement with [*I*,*I*-bis(trifluoroacetoxy)iodo] benzene (PIFA) in a DMSO and water mixture. The rearrangement is typically performed in water and the desired amine is obtained as hydrochloride from the aqueous layer [21,22]; especially for unpolar compounds the reaction lead to small yields [23]. The used cosolvent dissolved the azobenzeneglycineamide **8** and provided water which is required for the decarbonylation to the amine. Finally, the maleimide group was introduced similar to Scheme 1.

4.2. Bioconjugation of AMD **1a–e** to HDAH

The molar ratio of the average number of conjugated AMD molecules per each HDAH variant M30C molecule was determined by degree of labeling (DOL) experiments as described in the Materials and Methods section. The bioconjugation of AMDs to HDAH M30C is shown graphically in Fig. 1 and was experimentally verified by UV/Vis spectroscopy (see supplementary material Fig. A.1, *cis*/*trans* configuration). AMDs **1a–d** could be coupled to the HDAH variant M30C by Michael addition in a 1:1 M ratio, which corresponded to previous work [7] where the conjugation of 4-PAM was reported. The more hydrophobic AMD **1e** (n = 6) yielded a decreased DOL-value of 0.8 (see supplementary material Table A.1), which was slightly lower than expected. However after bioconjugation of **1e** to HDAH variant M30C the enzyme activity was almost completely abolished.

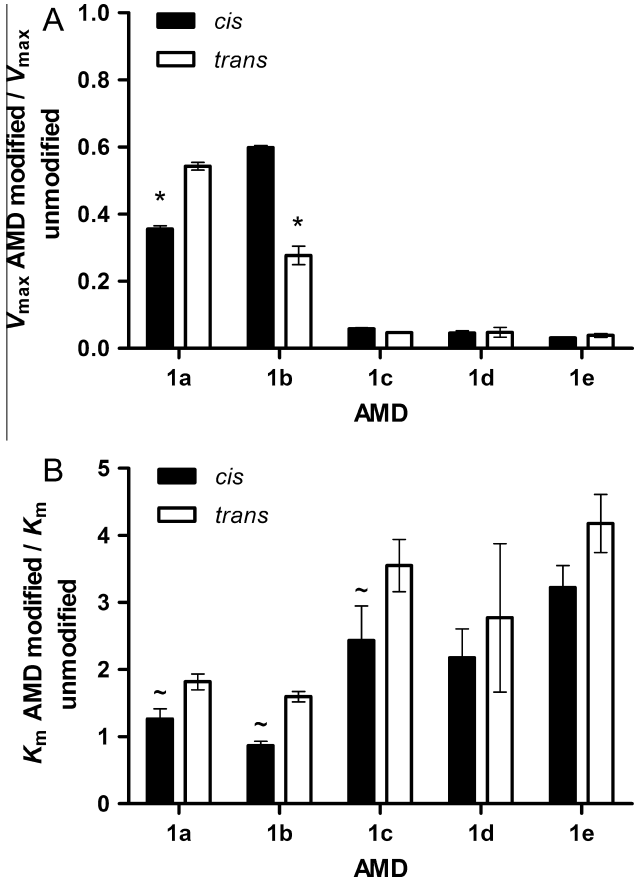

Fig. 3. Alkyl spacer dependent influence on Michaelis–Menten parameters of AMD/HDAH M30C conjugates concerning *cis*- and *trans*-configurations. Michaelis–Menten kinetics were performed and analyzed as described in the Materials and Methods section. V_{max} (A) and K_m (B) values of the *cis*- and *trans*-configuration for each tested AMD/HDAH M30C conjugate were respectively represented as relative ratios of the AMD modified and corresponding unmodified HDAH M30C variant. Values are means ± SD, n = 3. Statistical analysis for V_{max} and K_m values were performed by using one-way ANOVA with Bonferroni post hoc test. $^aP < 0.05$ (*cis* AMD vs. *trans* AMD). * = V_{max} – photoswitchable AMD/HDAH M30C variant conjugate. ~ = K_m – photoswitchable AMD/HDAH M30C variant conjugate.

4.3. Michaelis–Menten kinetics

The influence of the AMD spacer length with respect to the *cis*- and *trans*-configuration was investigated by Michaelis–Menten kinetics. V_{max}- and K_m-values of the respective *cis*- and *trans*-isomer of AMD (**1a–e**) modified HDAH M30C variants were calculated relative to the corresponding unmodified HDAH M30C sample (Fig. 3 A and B). The half-life of the *cis*-configuration was estimated to be at least 30 h for HDAH M30C/4-PAM [7] and HDAH M30C/**1e** conjugates. The required time to perform the corresponding irradiation of the samples and to measure Michaelis–Menten kinetics is accomplished within 80 min. Therefore, the relaxation did not influence the enzyme kinetics. The bioconjugation of AMD **1a** and **b** to HDAH M30C enabled a photoswitching of the rate of product formation over a broad range of substrate concentrations (Fig. 2A and B). During the past three decades, the ratio k_{cat}/K_m or V_{max}/K_m was frequently used to compare the catalytic efficiency of different enzymes, e.g. mutated or otherwise modified, working on the same substrate. However, Eisenthal et al. [25] clearly argued that, the use of k_{cat}/K_m as a quantitative index for catalytic effectiveness of enzymes is not only flawed, but also misleading in many cases. Even if an enzyme has a higher k_{cat}/K_m ratio, it can catalyze the same reaction at lower rates than another enzyme (at the same concentration $[E]_0$) with lower k_{cat}/K_m ratio at certain substrate concentrations, $[S]$. Generally, neither the use of k_{cat}/K_m nor simply V_{max} or K_m enables a fair comparison of two enzymes at all substrate concentrations. Therefore, in this study both Michaelis parameters, $V_{max} = k_{cat} \times [E]_0$ and K_m, and their effect on the rate of product formation where analyzed separately. The change in V_{max} turned out to have a more profound effect on the rate of the enzyme reaction than a change in K_m. The relative change in the product formation rates upon photoswitching from the *trans*- to the *cis*-configuration of the azobenzene moiety depends on $[S]$ (Fig. 2C and D). This demonstrates that the rate of the enzyme reaction, which can be calculated using V_{max}, is the decisive index to compare the effectiveness of two enzyme activities on the same substrate concentration. In our case the enzyme conjugate with AMD **1a** in *trans*-configuration catalyzed the reaction more effectively than the corresponding *cis*-configuration at all substrate concentrations. In contrast, the enzyme reaction of the *trans*-AMD **1b** enzyme conjugate occurred at lower rates compared with its *cis*-analog at all substrate concentrations. The photoisomerization from the *trans*- to the *cis*-configuration of AMD **1a** decreased the V_{max}-value significantly by 35% whereas V_{max} of the AMD **1b** conjugate was decreased by 54% upon *cis*–*trans* photoswitching (Fig. 3A). Furthermore it could be observed that the K_m-values of AMDs **1a** (44%) and **1b** (84%) were significantly increased by *cis*-to-*trans* isomerization (Fig. 3B). The attachment of AMDs **1c–e** with an alkyl spacer length of $\geqslant 3$ methylene groups led to an almost complete inhibition of the HDAH M30C conjugate in both configurations (residual activity < 6%) (Fig. 3A). By this reason its enzyme activity could not be photoswitched. The K_m-value of HDAH M30C was, compared to AMD **1a–b**, increased by AMD **1c–e** to a higher extent. Regarding the photoswitch behavior of the K_m-values of AMD **1c–e**, only AMD **1c** showed a significant alteration due to *cis*-to-*trans* isomerization (43%). Determined V_{max}- and K_m-values were summarized in Table A.2 (see supplementary material) and performed Michaelis–Menten kinetics represented in Fig. A.2.

On the basis of both verified Michaelis–Menten parameters (V_{max} and K_m), AMDs with varying spacer length showed distinct effects on the HDAH variant M30C enzyme activity and the ability to switch V_{max}- and K_m-values by irradiation. Conjugation of AMDs (**1d** and **e**) led to an almost complete inhibition of the enzyme

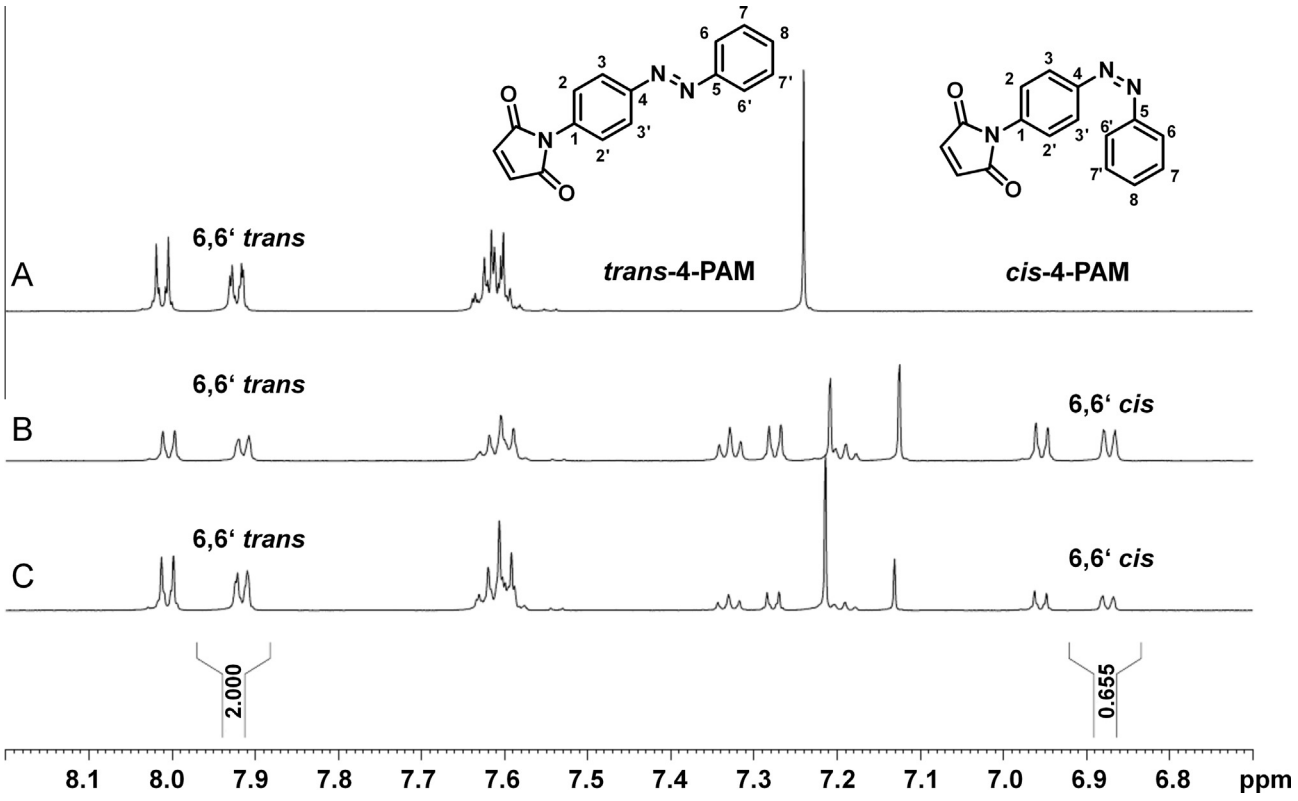

Fig. 4. 600 MHz ^{1}H NMR spectra of 4-PAM in DMSO-d_6. 5 mM 4-PAM/DMSO-d_6 solutions were treated differently. (A) incubation at 80 °C for 1 h; (B) 25 min, 364 nm; (C) 25 min, 464 nm. ^{1}H NMR spectroscopy was performed as described in the supplementary material. The annotation of 6 and 6′ protons of *cis*- and *trans*-4-PAM for PSS calculation is indicated by integral values. For analysis and quantification of PSS for 4-PAM, please see Table A.4.

whereas short spacer AMDs (**1a** and **b**) had a moderate influence on the activity. Therefore, they are able to control the protein function due the variation of the configuration. Determined V_{max}- and K_m-values for the AMD **1b**/HDAH M30C conjugate coincide very well. The photoisomerization to *cis* (catalytic more active enzyme) led to a decrease and the isomerization to *trans* (more inactive enzyme) to an increase of the K_m-value (Fig. 3A and B), which corresponds also to previously published work [7]. In comparison to AMD **1b,** AMD **1a** showed an inverse photoswitching behavior where the *trans*-isomer enabled the more active form of the enzyme conjugate. The observation that the *trans*-isomer of AMD **1a** showed a higher K_m-value but also a higher V_{max}-value could be explained by a scenario where *cis* **1a** blocks the active site more sterically than the *trans*-isomer but does not initiate large conformational changes at the enzyme or a decrease of the substrate affinity. In contrast, the more hydrophobic *trans*-isomer could induce a more pronounced distortion of the active site. This suggestion could explain the significant differences for the *cis*- and *trans*-isomer in the observed photoswitching behavior of **1a** and **b** conjugates.

4.4. Determination of the photostationary state (PSS) of 4-PAM

For the evaluation of the actual photoswitching efficiency of AMD/HDAH M30C conjugates, we measured the PSS of 4-PAM, the shortest employed maleimide azobenzene derivate, by ^{1}H NMR spectroscopy in DMSO-d_6 (Fig. 4). A blue light irradiation (464 nm) of 25 min resulted in a calculated *cis*-/*trans*-isomer ratio of 24.7/75.3%. In case of UV light irradiation (364 nm, 25 min) a *cis*-/*trans*-isomer ratio of 53.5/46.5% was calculated (Table A.4). Under the assumption, that the PSS behavior in DMSO could be transferred to the photoswitchable AMD **1a**- or **1b**-HDAH-M30C conjugates in water, the following theoretical V_{max} values were calculated for the 100% *cis*- or *trans*-isomers: 4.59 nM s^{-1} for the *trans*- and 0.35 nM s^{-1} for the *cis*-isomer of AMD **1a** as well as 0.02 nM s^{-1} for the *trans*- and 6.47 nM s^{-1} for the *cis*-isomer of AMD **1b**, respectively. This means that the enzyme activity of both, AMD **1a**- and **1b**-, conjugates would be theoretically switched more substantially by 92% and 99% upon complete photoconversion of the azobenzene group instead of the observed 35% and 54%. The experimental determination of PSS of 4-PAM and the AMDs conjugated to a HDAH variant dissolved in buffer, was not possible by NMR due to solubility and concentration issues.

4.5. Inhibition of the HDAH variant C51S

HDAH variant C51S was used to determine the IC_{50}-values of 4-PAM and AMDs in *cis*- and *trans*-configuration. No significant differences with respect to the enzyme activity could be found between the azobenzene derivatives (4-PAM and AMDs **1a–e**) and the respective configuration of the azobenzene group (see supplementary material Table A.3). All tested azobenzene derivatives showed only a weak (<10 μM) inhibition on the HDAH C51S enzyme activity and were at least 260 times less potent compared to a typical pan-inhibitor like SAHA (see supplementary material Fig. A.3 vs. Fig. A.3). The weak apparent inhibitory effect was mainly attributed to DMSO (see supplementary material Fig. A.3) which was used to prepare the stock solutions of the compound.

5. Conclusion

A novel series of photoswitchable maleimide derivatives was synthesized and covalently coupled to a specific variant of HDAH close to the active site. Depending on the configuration of azobenzene and the alkyl spacer length the enzyme activity (V_{max}) could be photocontrolled through two different mechanisms. In one case the *cis*-conjugate was more active, whereas in the other case the *trans*-conjugate showed a higher rate of product formation. Three AMD variants led to a complete inhibition of the enzyme in both azobenzene configurations. Even when a suitable position for the introduction of a cysteine in close proximity to the functional site of a protein could be identified from a crystal structure, the exact chemical structure of a conjugated photoswitch for optimal control of protein function is very hard to predict. We suggest the newly synthesized series of cysteine reactive AMDs as a general tool box to generate photoswitchable conjugates and enable a systematic exploration of the optimal intramolecular arrangement of the photoswitch with respect to the functional site. This approach should be applicable to other proteins, e.g. enzymes or ion channels, with cysteine residues at specified and solvent exposed positions on the protein surface.

Acknowledgments

This work was supported by a grant of the hessian Landes-Offensive zur Entwicklung Wissenschaftlich-ökonomischer Exzellenz (LOEWE Soft Control).

Appendix A. Supplementary material

Supplementary data associated with this article can be found, in the online version, at http://dx.doi.org/10.1016/j.bioorg.2014.10.004. These data include MOL files and InChiKeys of the most important compounds described in this article.

References

[1] I. Willner, S. Rubin, Angew. Chem., Int. Ed. Engl. 35 (1996) 367–385.
[2] C. Brieke, F. Rohrbach, A. Gottschalk, G. Mayer, A. Heckel, Angew. Chem., Int. Ed. 51 (2012) 8446–8476.
[3] W. Szymanski, J.M. Beierle, H.A. Kistemaker, W.A. Velema, B.L. Feringa, Chem. Rev. 113 (2013) 6114–6178.
[4] B. Schierling, A.-J. Noël, W. Wende, E. Volkov, E. Kubareva, T. Oretskaya, et al., Proc. Natl. Acad. Sci. 107 (2010) 1361–1366.
[5] W.-C. Lin, C.M. Davenport, A. Mourot, D. Vytla, C.M. Smith, K.A. Medeiros, et al., ACS Chem. Biol. (2014).
[6] T. Shimoboji, E. Larenas, T. Fowler, S. Kulkarni, A.S. Hoffman, P.S. Stayton, Proc. Natl. Acad. Sci. 99 (2002) 16592–16596.
[7] M. Korbus, G. Balasubramanian, F. Müller-Plathe, H. Kolmar, F.-J. Meyer-Almes, Biol. Chem. (2014) 401–412.
[8] J.H. Harvey, D. Trauner, ChemBioChem 9 (2008) 191–193.
[9] L. Chi, O. Sadovski, G.A. Woolley, Bioconjug. Chem. 17 (2006) 670–676.
[10] S.-L. Dong, M. Löweneck, T.E. Schrader, W.J. Schreier, W. Zinth, L. Moroder, et al., Chem.–Eur. J. 12 (2006) 1114–1120.
[11] D. Hoersch, S.-H. Roh, W. Chiu, T. Kortemme, Nat. Nanotechnol. (2013) 928–932.
[12] A.A. Beharry, G.A. Woolley, Chem. Soc. Rev. 40 (2011) 4422–4437.
[13] D. Bullock, C. Cumper, A. Vogel, J. Chem. Soc. (1965) 5316–5323.
[14] N. Stephanopoulos, M.B. Francis, Nat. Chem. Biol. 7 (2011) 876–884.
[15] P. Gorostiza, M. Volgraf, R. Numano, S. Szobota, D. Trauner, E.Y. Isacoff, Proc. Natl. Acad. Sci. 104 (2007) 10865–10870.
[16] R. Numano, S. Szobota, A.Y. Lau, P. Gorostiza, M. Volgraf, B. Roux, et al., Proc. Natl. Acad. Sci. 106 (2009) 6814–6819.
[17] D. Wegener, C. Hildmann, D. Riester, A. Schwienhorst, Anal. Biochem. 321 (2003) 202–208.
[18] D. Wegener, F. Wirsching, D. Riester, A. Schwienhorst, Chem. Biol. 10 (2003) 61–68.
[19] F.E. DeBons, G.M. Loudon, J. Org. Chem. 45 (1980) 1703–1704.
[20] R.H. Boutin, G.M. Loudon, J. Org. Chem. 49 (1984) 4277–4284.
[21] A.E. Sutton, J. Clardy, J. Am. Chem. Soc. 123 (2001) 9935–9946.
[22] A.E. Sutton, J. Clardy, Org. Lett. 2 (2000) 319–321.
[23] K.-S. Song, M.J. Kim, H.J. Seo, S.-H. Lee, M.E. Jung, S.-U. Kim, et al., Bioorg. Med. Chem. 17 (2009) 3080–3092.
[24] S. Schäfer, L. Saunders, E. Eliseeva, A. Velena, M. Jung, A. Schwienhorst, et al., Bioorg. Med. Chem. 16 (2008) 2011–2033.
[25] R. Eisenthal, M.J. Danson, D.W. Hough, Trends Biotechnol. 25 (2007) 247–249.